

Magnetic Excitations in Polyoxometalate Clusters Observed by Inelastic Neutron Scattering: Evidence for Anisotropic Ferromagnetic Exchange Interactions in the Tetrameric Cobalt(II) Cluster $[\text{Co}_4(\text{H}_2\text{O})_2(\text{PW}_9\text{O}_{34})_2]^{10-}$. Comparison with the Magnetic and Specific Heat Properties

Hanspeter Andres,[†] Juan M. Clemente-Juan,[‡] Michael Aebbersold,[†] Hans U. Güdel,^{*,†} Eugenio Coronado,^{*,‡} Herma Büttner,[§] Gordon Kearly,[§] Julio Melero,^{||} and Ramón Burriel^{||}

Contribution from the Departement für Chemie und Biochemie, Universität Bern, Freiestrasse 3, 3000 Bern 9, Switzerland, Departamento de Química Inorgánica, Universidad de Valencia, Dr. Moliner 50, 46100 Burjassot, Spain, Institut Laue Langevin, Avenue des Martyrs, B. P. 156, F-38042 Grenoble Cedex 9, France, and Instituto Ciencia Materiales de Aragón, CSIC-Universidad de Zaragoza, 50009 Zaragoza, Spain

Received January 20, 1999

Abstract: The ground-state properties of the tetranuclear Co^{2+} cluster $[\text{Co}_4(\text{H}_2\text{O})_2(\text{PW}_9\text{O}_{34})_2]^{10-}$ were investigated by combining specific heat, magnetic susceptibility, and magnetization measurements with a detailed inelastic neutron scattering (INS) study on a fully deuterated sample of $\text{K}_{10}[\text{Co}_4(\text{H}_2\text{O})_2(\text{PW}_9\text{O}_{34})_2] \cdot 22\text{H}_2\text{O}$. As a result of the single ion anisotropy of the octahedral Co^{2+} , the appropriate exchange Hamiltonian of the Co_4 spin cluster is anisotropic. INS turns out to be essential for the determination of energy splittings in the ground state resulting from the coupling. Besides the energy pattern, INS provides information about the wave functions of the split ground-state components of the spin cluster. Based on the Hamiltonian $\hat{H}_{\text{AN}} = \sum_{i=x,y,z} -2J_i(S_1iS_3i + S_1iS_4i + S_2iS_3i + S_2iS_4i) - 2J'_i(S_1iS_2i)$ the following set of parameters is obtained: $J_z = 1.51$ meV, $J_x = 0.70$ meV, $J_z' = 0.46$ meV, $J_x' = 0.44$ meV, $r = 1.6$, where $r = J_x/J_y = J_x'/J_y'$. These parameters also reproduce the magnetic specific heat, susceptibility, and magnetization properties of the compound.

Introduction

As we have pointed out in the preceding paper, polyoxometalates constitute ideal models for the study of exchange interactions in magnetic clusters.¹ In these metal–oxide molecular clusters, a variety of physical techniques, including the spectroscopic technique of inelastic neutron scattering (INS), can be used to determine the energies and wave functions of the different spin states of the cluster. This technique has been applied to a variety of exchange coupled clusters and proved to provide a much deeper and more detailed insight into the nature of the magnetic coupling than bulk techniques such as magnetic susceptibility and magnetic specific heat.² The title compound contains a tetramer cluster of cobalt (II) encapsulated by two heptadentate tungstophosphate ligands $[\text{PW}_9\text{O}_{34}]^{9-}$. It has the same geometry as the Ni_4 cluster in ref 1. The four Co^{2+} ions are octahedrally coordinated and all lie in one plane

forming a rhomblike tetramer structure. In this case, the difficulties associated with the exchange topology of the cluster, already emphasized in the analogous Ni(II) cluster, are accentuated by the fact that the exchange interactions are expected to be anisotropic due to the highly anisotropic ground state of octahedral Co(II). Although the magnetic properties were useful to prove that the overall exchange coupling is ferromagnetic, they failed in providing any information about the degree of exchange anisotropy and the two types of exchange pathways present in the cluster.³

Here we will tackle this problem with a high-resolution INS study of a fully deuterated sample of the salt $\text{K}_{10}[\text{Co}_4(\text{H}_2\text{O})_2(\text{PW}_9\text{O}_{34})_2] \cdot 22\text{H}_2\text{O}$. As suggested by preliminary INS studies, an anisotropic exchange model is required to describe the exchange coupling in this cluster.⁴ In the present paper, we resolve the individual magnetic excitations and study their scattering intensities as a function of temperature and scattering vector \mathbf{Q} . This will enable us to determine not only the energy splitting of the ground state but also the wave functions of the various ground state components. Reliable values for the exchange parameters will be derived, and it will be demon-

[†] Universität Bern.

[‡] Universidad de Valencia.

[§] Institut Laue Langevin.

^{||} Instituto Ciencia Materiales de Aragón.

(1) Clemente-Juan, J. M.; Andres, H.; Aebbersold, M.; Borrás-Almenar, J. J.; Coronado, E.; Güdel, H. U.; Büttner, H.; Kearly, G. *J. Am. Chem. Soc.* **1999**, *121*, 10021–10027.

(2) (a) Güdel, H. U.; Furrer, A. *Mol. Phys.* **1977**, *5*, 1335. (b) Güdel, H. U. In *Magneto structural correlations in exchange coupled systems*; Willett, R. D., Gatteschi, D., Kahn, O., Eds.; NATO ASI Series C 140; D. Reidel Publishing Company: Dordrecht, 1985; pp 329–354. (c) Güdel, H. U. In *Molecular Magnetism: From Molecular Assemblies to the devices*; Coronado, E., Delhaès, P., Gatteschi, D., Miller, J. S., Eds.; NATO ASI Series E 321; Kluwer Academic Publishers: Dordrecht, 1996; pp 229–242.

(3) (a) Casañ-Pastor, N.; Bas-Serra, J.; Coronado, E.; Pourroy, G.; Baker, L. C. K. *J. Am. Chem. Soc.* **1992**, *114*, 10380. (b) Gómez-García, C. J.; Coronado, E.; Borrás-Almenar, J. J. *Inorg. Chem.* **1992**, *31*, 1669.

(4) (a) Gómez-García, C. J.; Coronado, E.; Borrás-Almenar, J. J.; Aebbersold, M.; Güdel, H. U.; Mutka, H. *Physica B* **1992**, *181*, 238. (b) Clemente, J. M.; Andres, H.; Aebbersold, M.; Borrás-Almenar, J. J.; Coronado, E.; Güdel, H. U.; Büttner, H.; Kearly, G. *Inorg. Chem.* **1997**, *36*, 2244.

strated, for the first time, that an anisotropic exchange Hamiltonian acting on the basis of effective spins $s = 1/2$ is a convenient approach to model the exchange interactions between octahedrally coordinated Co(II) ions. Support for this anisotropic model will be provided by the results of magnetic and specific heat measurements.

Experimental Section

Synthesis. Full deuteration of the sample is required for INS experiments due to the large incoherent neutron cross section of the hydrogen atom. All physical measurements reported here were performed on this deuterated sample. An amount of ca. 30 g of the salt $K_{10}[Co_4(H_2O)_2(PW_9O_{34})_2] \cdot 22H_2O$ was obtained following the procedure described in the literature.⁵ The product was subsequently twice recrystallized from D_2O and characterized by chemical analysis, infrared spectroscopy, and X-ray powder diffraction using the program LAZY PULVERIX⁶ and the structural data given in ref 7.⁷ Around 20 g of the polycrystalline fully deuterated sample was then sealed under helium in an aluminum container of 15 mm diameter and 55 mm length suitable for INS experiments.

Inelastic Neutron Scattering. INS spectra with cold neutrons were recorded on the time-of-flight spectrometer IN6 at the Institut Laue Langevin (ILL) in Grenoble. The measurements were performed at temperatures of 1.7, 10, and 30 K with incident neutron wavelengths of 4.1 and 5.9 Å. The data treatment involved the subtraction of a background spectrum using an empty aluminum container of the same size and the calibration of detectors by means of a spectrum of vanadium metal. The time-of-flight to energy conversion and the data reduction were done with the standard program INX at the ILL. Further data treatment was done using the commercial program Igor (WaveMetrics).

Magnetic Measurements. Variable-temperature susceptibility measurements were carried out in the temperature range 2–300 K at a magnetic field of 0.1 T using a magnetometer (Quantum Design MPMS-XL-5) equipped with a SQUID sensor. Isothermal magnetization measurements as a function of the external magnetic field were performed up to 5 T at 2 and 5 K.

Heat Capacity. The heat capacity of well crystallized sample grains was measured in a Termis⁸ adiabatic calorimeter from 2.5 to 120 K. An amount of 2.6 g of the Co_4 cluster compound was sealed in the 1 cm³ sample container with 28 mbar of helium gas to ensure heat exchange and temperature equilibrium. The measurements were made with temperature steps between 0.5 and 1.5 K. Carbon-glass and Rh–Fe thermometers were used on the sample holder and on the adiabatic shield that surrounds it, being controlled at the temperature of the sample to provide adiabatic conditions. The sample specific heat was obtained after subtracting the empty sample holder contribution measured in a separate experiment. Similar measurements were done on 2.0 g of the isostructural Zn_4 cluster compound to deduce the nonmagnetic lattice specific heat.

Results

Inelastic Neutron Scattering. In Figure 1, we report the INS spectra of a polycrystalline sample of $K_{10}[Co_4(D_2O)_2(PW_9O_{34})_2] \cdot 22D_2O$ obtained with an incident neutron wavelength of 4.1 Å at three temperatures. They cover an energy region up to 3.8 meV⁹ on the neutron energy loss side with a resolution of 170 μ eV. Below 1.2 meV, these spectra are slightly obscured by a spurious peak around 0.8 meV, most probably a Bragg reflection of the aluminum-shielded cryostat. The onset of this excitation is designated by Al in Figure 1. The 1.7 K spectrum can be

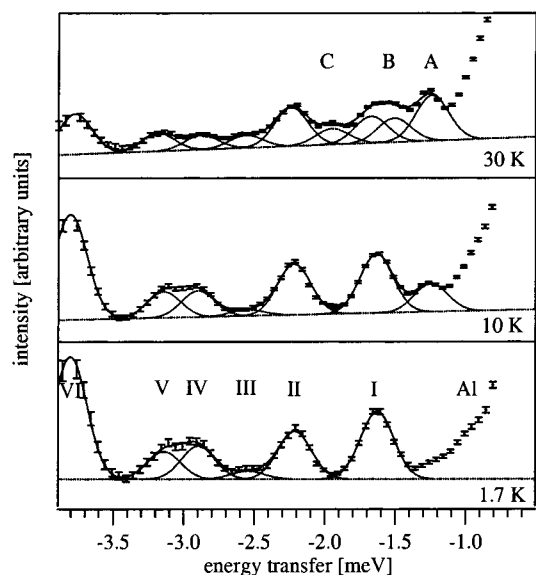


Figure 1. Neutron energy loss INS spectra of polycrystalline $K_{10}[Co_4(D_2O)_2(PW_9O_{34})_2] \cdot 22D_2O$ measured on the IN6 spectrometer with an incident neutron wavelength of 4.1 Å. The experimental points are shown for the three temperatures $T = 1.7$ K (bottom), 10 K (middle) and 30 K (top) with inclusion of least-squares Gaussian fits with equal widths. Cold transitions are labeled I–VI and hot transitions A–C, respectively.

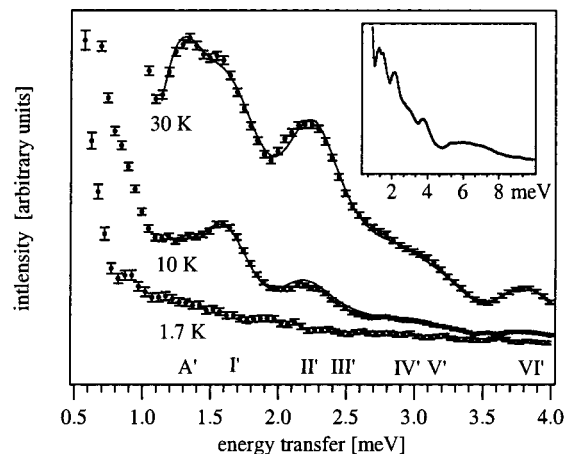


Figure 2. Neutron energy gain INS spectra of polycrystalline $K_{10}[Co_4(D_2O)_2(PW_9O_{34})_2] \cdot 22D_2O$ measured on the IN6 spectrometer with an incident neutron wavelength of 4.1 Å. The experimental points are shown for three temperatures $T = 1.7$, 10, and 30 K with inclusion of least-squares Gaussian fits as solid lines. Primed labels of the corresponding transitions on the loss side are used. The inset shows a 30 K spectrum up to 10 meV.

reproduced with a linear background and six Gaussians I–VI of equal width centered at 1.63, 2.21, 2.47, 2.92, 3.14, and 3.80 meV, as seen by the dotted lines in the bottom spectrum of Figure 1. At 10 and 30 K, the hot transitions A–C at 1.27, 1.51, and 1.95 meV can be identified, as seen in the upper two spectra of Figure 1. All these transitions are also observed although less resolved on the neutron energy gain side of the spectrum at elevated temperatures. This is shown in Figure 2, primed labels are used for corresponding transitions to Figure 1. The absence of the Al peak at 0.8 meV in the energy gain spectrum proves its spurious nature in the loss spectrum. On the energy gain side, unresolved magnetic excitations up to 10 meV can be observed at 30 K; see the inset of Figure 2.

In Table 1 we list positions and intensities of the various transitions as determined from the least-squares fits with

(5) Finke, R. G.; Droegge, M. W.; Domaille, P. J. *Inorg. Chem.* **1987**, *26*, 3886.

(6) Yvon, K.; Jeitschko, W.; Erwin, P. *J. Appl. Crystallogr.* **1977**, *10*, 73.

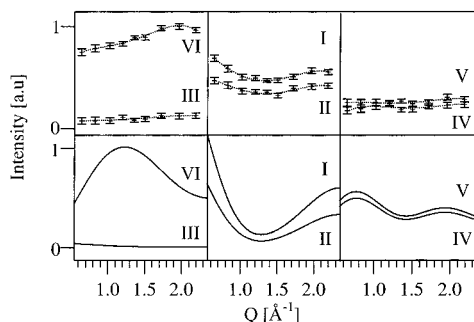
(7) Weakley, T. J. R.; Evans, H. T.; Showell, J. S.; Tourné, G. F.; Tourné, C. M. *J. Chem. Soc., Chem. Commun.* **1973**, 139.

(8) Pavese, F.; Malyshev, V. M. *Adv. Cryog. Eng.* **1994**, *40*, 119.

(9) The common energy unit in neutron scattering is 1 meV = 8.0655 cm⁻¹.

Table 1. Experimental Intensities with Estimated Errors of the Various INS Transitions for Neutron Energy Gain and Loss

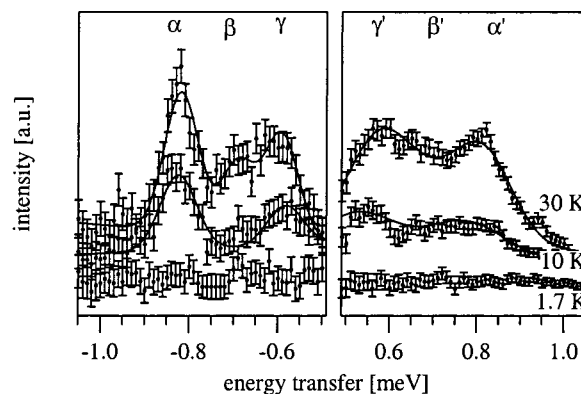
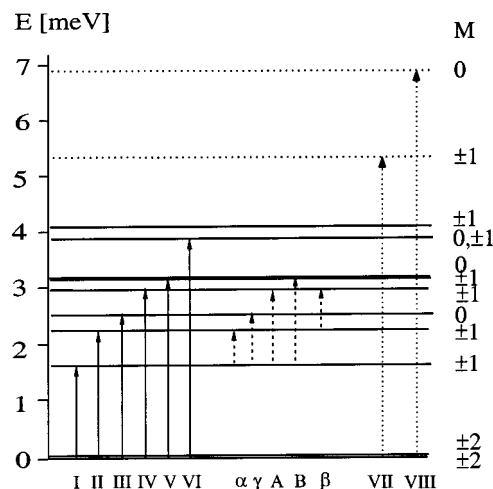
energy label	energy [meV]	intensity [au]				
		energy loss		energy gain		
		1.7 K	10 K	30 K	10 K	30 K
α	0.58	0.30 ± 0.05	0.7 ± 0.1	0.10 ± 0.07	0.81 ± 0.08	
β	0.69		0.54 ± 0.08		0.66 ± 0.06	
χ	0.82	0.67 ± 0.06	1.2 ± 0.1	0.24 ± 0.07	1.06 ± 0.05	
A	1.27	7.7 ± 0.4	12.2 ± 0.4	1.94 ± 0.05	7.5 ± 0.2	
B	1.51		4.9 ± 0.4			
I	1.63	18.8 ± 0.7	15.9 ± 0.3	7.2 ± 0.4	2.92 ± 0.05	
C	1.95		3.0 ± 0.4			
II	2.21	13.3 ± 0.6	13.8 ± 0.5	10.4 ± 0.4	1.41 ± 0.04	
III	2.47	2.2 ± 0.5	1.7 ± 0.3	3.4 ± 0.3	0.42 ± 0.03	
IV	2.92	9.2 ± 0.7	7.1 ± 0.3	3.9 ± 0.3	0.32 ± 0.03	
V	3.14	7.7 ± 0.6	7.0 ± 0.4	4.9 ± 0.3	1.2 ± 0.2	
VI	3.80	34 ± 1	28.9 ± 0.8	10.9 ± 0.4	1.7 ± 0.3	
VII	5.3					
VIII	6.7					

**Figure 3.** (Top) Intensities of transitions I–VI as a function of the scattering vector Q as obtained from least-squares Gaussian fits in the 1.7 K spectrum of Figure 1. The dotted lines are guides to the eye. (Bottom) Calculated intensity behavior of the transitions I–VI as a function of Q on the basis of the coupled cluster wave functions in Table 3. The intensities were normalized to the maximum of transition VI.

Gaussians shown in Figures 1 and 2 for neutron energy loss and gain, respectively, as a function of temperature. All the cold transitions show a clear decrease in intensity with increasing temperature on the loss side, except the weak transition III which coincides with a hot transition at 30 K. On the gain side, the overall intensity is an order of magnitude smaller so that only the intensities of the most intense peaks can be adequately determined. The observed behavior of all these excitations with temperature clearly identifies them as magnetic.

The good statistics of the 1.7 K spectrum enabled us to study the behavior of the scattering intensities of transitions I–VI as a function of the scattering vector Q . The result is plotted in the upper traces of Figure 3. We observe an intensity decrease between 0.8 and 1.4 \AA^{-1} for transitions I and II, before rising to a maximum at 2.1 \AA^{-1} , whereas transition VI continuously rises to a maximum at 2 \AA^{-1} . The remaining three transitions III, IV, and V have less pronounced Q dependencies, a characteristic sign for anisotropic exchange coupling. Overall, the observed Q dependence is another proof for the magnetic character of these transitions. Phonon excitations typically show an increase of INS intensity proportional to Q^2 .

To better resolve the region below 1.2 meV, we measured with a higher neutron wavelength of 5.9 \AA . These INS spectra are plotted in Figure 4 for three temperatures. At 1.7 K, no inelastic transition is observed in the energy transfer range 0.5–1.2 meV, whereas at elevated temperatures three hot transitions α , β , and γ at 0.58, 0.69, and 0.82 meV, respectively, are seen both in energy loss and gain. They were fitted with three

**Figure 4.** INS energy loss and gain spectra of the title compound at $T = 1.7, 10,$ and 30 K with an incident neutron wavelength of 5.9 \AA . Gaussian fits are included as solid lines. The labeling of the transitions is given at the top.**Figure 5.** Energy level diagram of the Co_4 cluster ground state derived from the INS experiments. Cold and hot transitions observed in the present study on the instrument IN6 are given as full and broken lines, respectively. The transitions and levels identified in an earlier study^{4a} on the instrument IN4 are given as dotted lines. The labels of the transitions are those used in Figures 1, 2, and 4. Each energy level is labeled according to the M value associated with the basis function having the leading contribution to the tetramer eigenfunction.

Gaussians of equal width; see the full lines in Figure 4. For these fits, the spectrum measured at 1.7 K was subtracted. The resulting energies and intensities of the transitions α – γ are included in Table 1.

From the experimental data presented in Figures 1, 2, and 4 and Table 1, we can derive the energy level diagram depicted in Figure 5. The cold transitions I–VI, shown as full arrows, all originate in the cluster ground state. Hot transitions, shown as broken arrows all originate in the excited levels at 1.63 and 2.21 meV. This energy level diagram agrees very well with a preliminary one based on low-resolution INS spectra.^{4a} The higher resolution of the present experiment enables us to show that the broad features at 2.2 and 2.9 meV reported in ref 4a both deconvolute into two transitions. Additional magnetic transitions at 5.3 and 6.7 meV were found in this earlier thermal neutron experiment, which was performed on the instrument IN4. We include these excitations and cluster levels by dotted arrows and lines in Figure 5.

Magnetic and Specific Heat Measurements. Magnetic susceptibility measurements on a polycrystalline sample in the range 2–30 K are shown in the inset of Figure 6 as a plot of the product χT vs T . χT shows a continuous increase upon

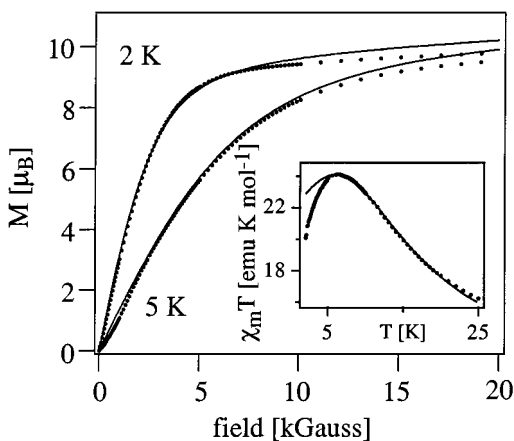


Figure 6. Experimental magnetization curves are presented for 2 and 5 K. The product χT versus T between 2 and 25 K for $K_{10}[Co_4(D_2O)_2(PW_9O_{34})_2] \cdot 22D_2O$ is shown in the inset. The best fits to the experimental data are shown as solid lines. They correspond to the exchange parameters derived from INS in eq 6 and $g_{\text{all}} = 6.0$, $g_{\text{a}\perp} = 5.1$, $g_{\text{b}\parallel} = 7.4$, $g_{\text{b}\perp} = 2.3$.

cooling reaching a rounded maximum around 6 K. This behavior is indicative of ferromagnetic Co(II)–Co(II) interactions. To get complementary information on the lowest lying levels of this cluster, isothermal magnetization curves were measured as a function of the applied magnetic field at 2 and 5 K. The results are shown in Figure 6. The results of the heat capacity measurements are shown up to 20 K in Figure 7. The heat capacity of the isostructural $K_{10}[Zn_4(H_2O)_2(PW_9O_{34})_2] \cdot 22H_2O$ which coincides with the values of the title compound at high temperatures and shows a smooth T^3 behavior below 20 K has been subtracted. The magnetic contribution of the title compound thus obtained shows a Schottky anomaly with a maximum of $1.45R^{10}$ at 10 K, as seen in Figure 7. The broad maximum occurs at slightly higher temperature than for the susceptibility.

Analysis and Discussion

Anisotropic Exchange Model. Encapsulation of the four Co^{2+} ions by two $[PW_9O_{34}]^{9-}$ ligands leads to a tetrameric rhomblike centrosymmetrical cluster Co_4O_{16} of D_{2h} symmetry formed by four coplanar edge-sharing CoO_6 octahedra. The structure is shown in Figure 1 of the preceding article.¹ The two dominant exchange pathways J and J' correspond to the interactions along the edges and the short diagonal of the rhomb, respectively. The 4T_1 ground state of octahedral Co^{2+} shows a first-order spin–orbit splitting. Considering the actual C_1 symmetry at the Co^{2+} sites, 4T_1 splits into six anisotropic Kramers doublets. The previous INS study using thermal neutrons showed that the first excited Kramers doublet lies above 14 meV.^{4a} Thus, at temperatures below 30 K, only the ground Kramers doublet is significantly populated. Magnetic susceptibility and EPR results clearly indicate the anisotropic nature of this Kramers doublet.^{3b} We can therefore attempt to describe the coupling in the tetramer by the pairwise coupling of highly anisotropic Kramers doublets with fictitious spin 1/2.¹¹ Expressing the single ion anisotropy in terms of the exchange anisotropy

(10) $R = 8.3144 \text{ J mol}^{-1} \text{ K}^{-1}$.

(11) (a) Ginsberg, A. P. *Inorg. Chim. Acta* **1971**, 45. (b) Lines, M. E. *J. Chem. Phys.* **1971**, 55, 2977.

(12) de Jongh, L. J.; Miedema, A. R. In *Experiments on simple magnetic model systems*; Coles, B. R., Eds.; Monographs on Physics; Taylor & Francis LTD: London, 1974; pp 1–269.

(13) Güdel, H. U.; Hauser, U.; Furrer, A. *Inorg. Chem.* **1979**, 18, 10. Güdel, H. U.; Furrer, A.; Murani, A. *J. Magn. Magn. Mater.* **1980**, 15–18, 383.

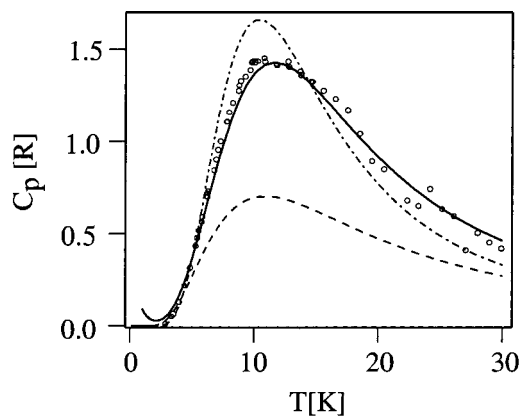


Figure 7. Experimental magnetic heat capacity data (open circles) for the title compound. The solid line is the calculated curve using the exchange parameters derived from INS in eq 6. The broken and dash-dotted lines represent the calculated heat capacity for the Heisenberg and Ising models, using the parameters $J = 0.93 \text{ meV}$, $J' = 0.31 \text{ meV}$ and $J_z = 1.30 \text{ meV}$, $J'_z = 0.43 \text{ meV}$, respectively.

we get the following effective Hamiltonian:¹²

$$\hat{H}_{\text{AN}} = \sum_{i=x,y,z} -2J_i(S_{1i}S_{3i} + S_{1i}S_{4i} + S_{2i}S_{3i} + S_{2i}S_{4i}) - 2J'_i(S_{1i}S_{2i}) \quad (1)$$

In eq 1, the subscripts 1/2 and 3/4 refer to the Co^{2+} ions separated by the short and long diagonal of the rhomb, respectively. We neglect the next-nearest neighbor interaction across the long diagonal. The operator (1) does not commute with \hat{S}^2 , the total spin of the cluster. Thus, it will mix the $|(S_{12})(S_{123})SM\rangle$ basis functions in eq 1, where S_{12} and S_{123} are intermediate spins defined as

$$S_1 + S_2 = S_{12}, \quad S_{12} + S_3 = S_{123}, \quad S_{123} + S_4 = S \quad (2)$$

The only valid quantum number for the cluster levels is M , and thus the tetramer eigenfunctions will be given by appropriate linear combinations of the $|(S_{12})(S_{123})SM\rangle$ basis functions:

$$\psi_n = \sum_{S_{12}, S_{123}, S, M} a_n(S_{12}, S_{123}, S, M) |(S_{12}, S_{123}, S, M)\rangle \quad (3)$$

where $a_n(S_{12}, S_{123}, S, M)$ are the eigenvector coefficients.

Analysis of the INS Results. We can test the ability of the anisotropic exchange Hamiltonian in eq 1 to reproduce the low-lying energy pattern derived from INS. In the most general case, this exchange model involves six adjustable parameters (the three components of the two exchange interactions J and J'). To reduce this number, we assume in a first approximation an axial anisotropy, i.e., $J_x = J_y = J_{xy}$ and $J'_x = J'_y = J'_{xy}$. This model provides an excellent reproduction of the experimental energy pattern in Figure 5 with the four parameters $J_z = 1.26 \text{ meV}$, $J_{xy} = 0.52 \text{ meV}$, $J'_z = 0.50 \text{ meV}$, and $J'_{xy} = 0.11 \text{ meV}$. In Table 2, we compare the experimental energy levels with the calculated ones; the corresponding wave functions are also given. Both interactions turn out to be ferromagnetic and anisotropic, with $J_z > J_{xy}$ and $J'_z > J'_{xy}$.

We can test the quality of the wave functions and thus the validity of this model by computing the INS intensities and comparing with the experimental values. For an analogous Cr_4^{3+} cluster with rhomblike geometry, the cross sections for the various types of transitions have been worked out.¹³ However, the present situation is complicated by the anisotropy and the purely isotropic formulas in ref 13 are insufficient. We make

Table 2. Experimental and Calculated Energy Levels with Corresponding Wavefunctions Expanded in the $|(S_{12})(S_{123})SM\rangle$ Basis Obtained for the Axial-Anisotropy Model

experimental energy [meV]	calculated energy [meV]	wave functions in $ (S_{12})(S_{123})SM\rangle$ basis
0.00	0.00	$ (1)(1.5)2\ 2\rangle$
1.63	1.66	$0.996 (1)(1.5)2\ \pm 1\rangle \pm 0.077 (1)(0.5)1\ \pm 1\rangle \pm 0.055 (1)(1.5)1\ \pm 1\rangle$
2.21	2.16	$-0.990 (1)(1.5)2\ 0\rangle + 0.143 (1)(0.5)0\ 0\rangle$
2.47	2.51	$\pm 0.816 (1)(1.5)1\ \pm 1\rangle \mp 0.577 (1)(0.5)1\ \pm 1\rangle$
2.90	2.91	$-0.816 (1)(1.5)1\ 0\rangle + 0.577 (1)(0.5)1\ 0\rangle$
3.14	3.12	$ (0)(1.5)1\ \pm 1\rangle, (0)(0.5)1\ 0\rangle, (0)(0.5)0\ 0\rangle$
3.80	3.76	$-0.095 (1)(1.5)2\ \pm 1\rangle + 0.813 (1)(0.5)1\ \pm 1\rangle + 0.575 (1)(1.5)1\ \pm 1\rangle$

use of the formalism developed by some of us¹⁴ which is of general validity. This formalism is based on the successive use of the irreducible tensor operator techniques, which allow us to take fully into account all kinds of magnetic exchange interactions between the metal ions comprised in clusters of arbitrary nuclearity and spin values, as well as the single ion anisotropic terms. The relevant cross section formula for a transition between two cluster levels ν and ν' is given by

$$\frac{\partial^2 \sigma}{\partial \Omega \partial \omega} = A \sum_{\nu, \nu'} \exp\left[-\frac{E(\nu)}{kT}\right] \sum_{\alpha, \beta} \left(\delta_{\alpha\beta} - \frac{Q_\alpha Q_\beta}{Q^2} \right) \times \sum_{m, n} F_m^*(\vec{Q}) F_n(\vec{Q}) \exp\{i\vec{Q}(\vec{R}_m - \vec{R}_n)\} \langle \nu | \hat{S}_m^\alpha | \nu' \rangle \times \langle \nu' | \hat{S}_n^\beta | \nu \rangle \delta(\hbar\omega + E_\nu - E_{\nu'}) \quad (4)$$

where $\alpha, \beta = x, y, z$; m and n number the magnetic ions within the cluster; $F_m(\vec{Q})$ is the magnetic form factor of Co^{2+} ; \vec{R}_m and \vec{R}_n are the position vectors of the Co^{2+} ions in the cluster. The quantity A is composed of a constant and the Debye–Waller factor as follows:

$$A = \frac{\gamma e^2}{m_e c^2} \frac{k'}{k} \exp(-2W)$$

Of particular relevance in eq 4 are the matrix elements of the form $\langle \nu | \hat{S}_m^\alpha | \nu' \rangle$ and the so-called interference factor $\exp\{i\vec{Q}(\vec{R}_m - \vec{R}_n)\}$. The latter leads to a modulation of the INS intensities reflecting the nearest-neighbor Co^{2+} – Co^{2+} distances in the cluster. The matrix elements are characterized by coupled cluster wave functions of the type in eq 3 and the spin operators acting on individual spins within the cluster. They are best evaluated by using tensor operator techniques.

We obtain, after proper integration over the measured Q range, the calculated relative intensities for transitions I–VI given in Table 3. In this table, the intensity of transition I was scaled to 1. We note that the proposed axial-anisotropic model completely fails in reproducing the intensity behavior, despite the excellent reproduction of the energy level pattern. In particular, within this model, zero intensity is calculated for transitions II and IV, while experimentally these have a non-negligible intensity, as seen in Figure 1. Qualitatively this result can be understood from a simple inspection of the cluster wave functions in Table 2 and the selection rules for magnetic INS.

(14) Borrás-Almenar, J. J.; Clemente-Juan, J. M.; Coronado, E.; Tsukerblat, B. S. Submitted.

(15) (a) Moira, T. *Phys. Rev.* **1960**, *120*, 91. (b) Levy, P. M. *Phys. Rev. Lett.* **1968**, *20*, 1366.

(16) In agreement with an EPR signal at a magnetic field of 100 G, Coronado E.; private communication.

Table 3. Comparison of the Normalized Experimental and Calculated Intensities for Transitions I–VI for Neutron-Energy Loss^a

label	energy [meV]	intensities			
		experimental	axial-anisotropy	antisymmetric	rhombic-anisotropy
I	1.63	1.00 ± 0.05	1.00	1.00	1.00
II	2.21	0.71 ± 0.04	0	10^{-4}	0.56
III	2.47	0.12 ± 0.03	0.81	0.81	0.04
IV	2.92	0.49 ± 0.04	0	10^{-4}	0.82
V	3.14	0.41 ± 0.04	0.75	0.75	0.69
VI	3.80	1.81 ± 0.09	0.72	0.73	1.39

^aThe third and fourth columns list the calculated intensities for axial-anisotropic exchange with and without 10% antisymmetric exchange, respectively, and column 5 lists the calculated intensities for the rhombic-anisotropy model with the parameters values in eq 6. The intensities were normalized to the value for transition I.

With M as the only quantum number to characterize the cluster levels, the following selection rules have to be considered:

$$\Delta M = 0, \pm 1 \quad (5)$$

are the only allowed INS transitions. As seen in Table 2, the axial-anisotropic model predicts a $M = \pm 2$ ground state. The levels II and IV have $M = 0$, and transitions are therefore forbidden.

We conclude that the above solution is not valid and we have to refine our effective Hamiltonian. With this aim we have explored in a first step the effect of an antisymmetric exchange,¹⁵ as it allows a further mixing of the coupled cluster wave functions. However, this model alters the situation only slightly, as seen by inspection of the calculated intensities in the corresponding column of Table 3. Even when the antisymmetric coupling constant is allowed to have the maximal value predicted by theory (10% of the isotropic coupling constant),¹⁵ the calculated intensities for transitions II and IV are still 4 orders of magnitude lower than the experimental ones.

The second possibility of refining the model is to drop the assumption of axial anisotropy. This makes physical sense, since it is the single-ion anisotropy which dictates the form of the effective exchange Hamiltonian. Neither of the two Co^{2+} sites is axial, and we allow the three components of J and J' in eq 1 to be different. This rhombic-anisotropy model is now capable of reproducing both the observed energies and relative intensities in a highly satisfactory way. Table 4 shows energies and wave functions corresponding to the best fit, and the last column of Table 3 shows the relative intensities. The exchange parameters thus derived are

$$J_z = 1.51 \text{ meV}, \quad J_x = 0.70 \text{ meV}, \quad J_z' = 0.46 \text{ meV}, \\ J_x' = 0.44 \text{ meV}, \quad r = 1.6 \quad (6)$$

Notice that we have reduced the number of adjustable parameters from six to five by setting $r = J_x/J_y = J_x'/J_y'$.

The relaxation of axial constraint in our model leads to additional energy splittings and significant modifications of the wave functions and thus the relative intensities. Both effects are seen in Table 4. The cluster ground state is now composed of a nearly degenerate doublet,¹⁶ the lower component of which is no longer a pure $M = \pm 2$ function but has some admixture of $M = 0$. For the excited levels, the energy shifts and splittings are more significant. In particular, the levels II and IV at 2.21 and 2.92 meV which, in the axial model, were not accessible from the ground level because of the selection rules, now have $M = \pm 1$ character and considerable intensities.

Table 4. Experimental and Calculated Energy Levels with Corresponding Wavefunctions Expanded in the $|(S_{12})(S_{123})S M\rangle$ Basis Obtained for the Rhombic-Anisotropy Model

experimental energy [meV]	calculated energy [meV]	wave functions in $ (S_{12})(S_{123})S M\rangle$ basis
0.00	0.00	$-0.699 (1)(1.5)2 2\rangle - 0.699 (1)(1.5)2 -2\rangle - 0.144 (1)(1.5)2 0\rangle$
	0.06	$-0.707 (1)(1.5)2 2\rangle + 0.707 (1)(1.5)2 -2\rangle$
1.63	1.68	$0.707 (1)(1.5)2 1\rangle + 0.707 (1)(1.5)2 -1\rangle$
2.21	2.28	$-0.970 (1)(1.5)2 0\rangle + 0.192 (1)(0.5)0 0\rangle + 0.105 (1)(1.5)2 2\rangle$
2.92	2.98	$0.408 (1)(0.5)1 \pm 1\rangle - 0.577 (1)(1.5)1 \pm 1\rangle$
3.14	3.14	$\pm 0.408 (1)(0.5)1 \pm 1\rangle \mp 0.408 (1)(1.5)1 \pm 1\rangle$
	3.17	$0.816 (1)(1.5)1 0\rangle - 0.577 (1)(0.5)1 0\rangle$
3.80	3.87	$ (0)(0.5)1 \pm 1\rangle$
	3.87	$ (0)(0.5)1 0\rangle$
	3.87	$ (0)(0.5)0 0\rangle$
	4.04	$-0.577 (1)(0.5)1 \pm 1\rangle - 0.408 (1)(1.5)1 \pm 1\rangle$
5.3	4.48	$\pm 0.577 (1)(0.5)1 \pm 1\rangle \mp 0.408 (1)(1.5)1 \pm 1\rangle$
	6.09	$-0.577 (1)(1.5)1 0\rangle - 0.814 (1)(0.5)1 0\rangle$
6.7	6.90	$-0.980 (1)(0.5)0 0\rangle$

A final test of the validity of this solution is provided by comparison of the experimental and observed Q dependencies of the INS intensities. Experimentally, we see in Figure 3 that the various transitions show differences in their Q dependence. Theoretically, there are 16 different Q dependencies for INS transitions between the pure $|(S_{12})(S_{123})S M\rangle$ basis functions according to the selection rules

$$\Delta S_{12} = 0, \pm 1, \quad \Delta S_{123} = 0, \pm 1, \quad \Delta M = 0, \pm 1 \quad (7)$$

By the mixing of these basis functions in the eigenfunctions of the cluster, these Q dependencies get scrambled. This scrambling is strongest in situations with large anisotropies. And the experimental behavior observed here clearly indicates such a situation. In Heisenberg systems, one observes much stronger Q dependencies of the magnetic cluster excitations than those shown for the title compound in Figure 3.¹⁷ The result obtained for the transitions I–VI using the wave functions in Table 4 is shown in the lower part of Figure 3. The overall agreement with experiment is fair. The observed Q dependencies are generally less pronounced than the calculated ones, but in all the trends are well reproduced. We interpret this as a confirmation of our model and the derived parameters. On the other hand, the remaining differences indicate that the wave functions are not yet perfect. The calculated Q dependencies are extremely sensitive to small changes in the wave functions.

Magnetic and Heat-Capacity Measurements. EPR measurements at 4.2 K on a codoped sample of the corresponding Zn compound showed as many as five signals indicating two different and anisotropic g tensors.^{3b} These are associated with the two types of Co^{2+} sites. Their g components are in the range 2.3–7.4. To fit the low-temperature magnetic susceptibility data, we fixed the exchange parameters obtained from INS and then allowed the anisotropic g parameters to vary in this range. To keep the number of parameters small, the two g tensors were assumed to be axial. A good fit that quantitatively reproduces both the increase in χT and its maximum at 6 K was obtained from the values $g_{a\parallel} = 6.0$, $g_{a\perp} = 5.1$, $g_{b\parallel} = 7.4$, $g_{b\perp} = 2.3$, where a and b represent sites 1/2 and 3/4, respectively. We note that below 5 K the calculated susceptibility deviates slightly from the experimental data. As expected, the hydrated sites 3/4 show a larger spin anisotropy. This different degree of spin anisotropy is in good agreement with the differences observed

in the anisotropy of the two exchange parameters. Thus, the exchange interaction involving the hydrated sites J , is more anisotropic than J' ($J_x/J_z = 0.46$; $J'_x/J'_z = 0.95$). Above 25 K, there is a deviation of the calculated susceptibility from the experimental data. We ascribe it to a population of higher Kramers doublets of Co^{2+} .

The proposed energy diagram, and in particular the nature of the ground state of the cluster, can be further tested by a low-temperature magnetization study performed as a function of the applied magnetic field at two different temperatures (2 and 5 K; see Figure 6). Using the computing procedure developed in ref 14, a nice reproduction of the experimental data is obtained with the exchange parameters derived by INS and the g values derived from magnetic susceptibility. There is no fit parameter in these calculated magnetization curves.

Finally, indirect information about the exchange anisotropy comes from the analysis of the specific heat measurements. This technique is very sensitive to the energy gap between the lowest lying levels of a magnetic system and to their degeneracy. In a plot of the temperature dependence of the magnetic heat capacity a rounded maximum is observed; its position is mainly determined by the first energy gap, while its height is sensitive to degeneracy. As the degeneracy of levels is directly connected with the type of exchange interactions, the height of the maximum will be the key feature to get information on the exchange anisotropy in the present Co_4 cluster. In Figure 7, we compare the magnetic heat capacity of the Co_4 cluster with the various exchange models. We note again that there is no adjustable parameter in the calculated curves. We observe that the rhombic-anisotropy exchange model derived from the INS study (full line) reproduces in a very satisfactory manner both the height and the position of the experimental maximum. In contrast, the fully isotropic Heisenberg model (broken line) is completely unable to account for the height of the maximum; it predicts a maximum heat capacity of $0.7R$, which is much lower than the experimental value at the maximum. The fully anisotropic Ising model (dash-dotted line) is closer to the experimental maximum. This is not surprising as this model leads to a degenerate spin doublet, $M = \pm 2$, for the ground state, which is similar to that predicted by our anisotropic exchange model derived from INS. However, the pure Ising model cannot reproduce the form of the experimental shape of the maximum. Another important conclusion from the heat capacity measurements is the absence of excited cluster levels between 0.2 and 1.65 meV, as demonstrated by the sharp decrease in C_p below 10 K, which is well reproduced by the model. This complementary information constitutes an additional support of the validity of the anisotropic exchange model and the resulting parameters derived from the INS results. Since no adjustable g values are involved, this support is more direct than for the magnetization and susceptibility measurements.

Conclusions

In those cases in which the constituent single ions of the clusters have no or a small single ion anisotropy, an isotropic Heisenberg model usually provides an adequate description of the energy splittings resulting from the magnetic interactions. Exchange parameters can then reliably be derived from the temperature dependence of the magnetic susceptibility. The situation is different when the constituent magnetic ions of the cluster exhibit a single ion anisotropy. The splitting pattern of the ground state becomes more complicated and the information content of the magnetic susceptibility is usually insufficient for its determination. The problem is a basic one: there is no model-

(17) (a) Güdel, H. U.; Furrer, A.; Blank, H.; *Inorg. Chem.* **1990**, *29*, 4081. (b) Furrer, A.; Güdel, H. U.; *Phys. Rev. Lett.* **1977**, *39*, 657.

independent way to determine a ground state splitting from bulk properties such as magnetic and specific heat data. In this situation, spectroscopic techniques can provide a valuable complement, because they allow a direct determination of these splittings. INS is particularly useful for the determination of exchange splittings because, in contrast to photon spectroscopy, $\Delta S = \pm 1$ transitions are also allowed.

The present Co_4 cluster is an illustrative example. The overall ferromagnetic nature of the exchange coupling is derived from the susceptibility, but the size and the anisotropy of the two competing interactions are determined by INS. The experimentally derived ground state splitting can be very well reproduced by an exchange Hamiltonian with purely axial anisotropy. But by considering the INS intensity in addition to their energies, this is found to be the wrong solution. At this point, the real strength of the INS technique becomes manifest. By way of the relative intensities and their Q dependence we get access to the wave functions of the coupled magnetic system. In the present case, we have to extend the anisotropy range, and with the rhombic-anisotropy model we finally obtain a set of parameters which is in agreement with both INS energies and intensities. In addition, these parameters reproduce the specific heat and magnetic susceptibility data, and we can be confident that both the model and the parameter values have some physical significance.

In Co_4 , the anisotropy has its origin in a first-order spin-orbit splitting of the 4T_1 ground state. In the Ni_4 cluster treated

in ref 1, the splitting of the 3A_2 ground state is a second-order effect. This leads to a significant difference in the appropriate exchange Hamiltonian. Whereas anisotropic exchange is essential for the description of the coupling in Co_4 , an isotropic Heisenberg model supplemented by a zero-field splitting term is sufficient in Ni_4 . On the experimental side, we note that for Co_4 the INS study was indispensable for the quantitative evaluation of the ground-state properties. For Ni_4 , the magnetic susceptibility and magnetization measurements contained enough information to place the $S = 4$ multiplet lowest in energy. For a quantitative evaluation of both the exchange and anisotropy parameters however, the INS experiments provided the relevant information. We conclude that the power of INS is greatest for exchange coupled systems composed of magnetic ions with a first or second-order single ion anisotropy.

Acknowledgment. This work has been developed in the framework of the European COST ACTION 518 (Project Magnetic Properties of Molecular and Polymeric Materials). Financial support by the Spanish Ministerio de Educación y Cultura (Grant PB96-0862) and the Swiss National Science Foundation are gratefully acknowledged. J.M.C-J. thanks the Generalitat Valenciana for a predoctoral grant.

JA990198R